OPEN

Fluorous Metal-Organic Frameworks with Enhanced Stability and High H$_2$/ CO$_2$ Storage Capacities

Da-Shuai Zhang[1], Ze Chang[1], Yi-Fan Li[2], Zhong-Yi Jiang[2], Zhi-Hong Xuan[1], Ying-Hui Zhang[1], Jian-Rong Li[3], Qiang Chen[1], Tong-Liang Hu[1] & Xian-He Bu[1]

[1]Department of Chemistry, Collaborative Innovation Center of Chemical Science and Engineering (Tianjin), and Tianjin Key Lab on Metal and Molecule-based Material Chemistry, Nankai University, Tianjin 300071, China, [2]Key Laboratory for Green Chemical Technology, School of Chemical Engineering and Technology, Tianjin University, Tianjin 300072, China, [3]College of Environmental and Energy Engineering, Beijing University of Technology, Beijing 100124, China.

A new class of metal-organic frameworks (MOFs) has been synthesized by ligand-functionalization strategy. Systematic studies of their adsorption properties were performed at low and high pressure. Importantly, when fluorine was introduced into the framework via the functionalization, both the framework stabilities and adsorption capacities towards H$_2$/CO$_2$ were enhanced significantly. This consequence can be well interpreted by theoretical studies of these MOFs structures. In addition, one of these MOFs TKL-107 was used to fabricate mixed matrix membranes, which exhibit great potential for the application of CO$_2$ separation.

H ydrogen storage and carbon dioxide capture have become two great challenges for the scientific world[1,2]. Many investigations have been focused on the synthesis of new porous materials, like carbon nanotubes, zeolites, metal-organic frameworks (MOFs) or porous coordination polymers (PCPs)[3–5], and porous organic frameworks for pursuing these issues[6–9]. Among these materials, MOFs have been widely studied in the past two decades[10]. The high crystallinity and porosity characteristics of MOFs materials make them potentially applicable to various domains, such as gas storage[11], separation[12–15], catalysis[16,17], luminescence[18–20], drug delivery[21,22], and so on. For gas adsorption properties, some MOFs have shown remarkable H$_2$ storage and CO$_2$ capture ability at high pressure due to their high porosity and large pore size[23,24]. However, to the best of our knowledge, there are only a small number of MOFs which exhibit over 2.0 wt% H$_2$ uptake at 77 K and 1 atm and over 100 cm^3 g^{-1} CO$_2$ uptake at 298 K and 1 atm so far. To enhance the adsorption performances of MOFs toward practical applications, several strategies have been developed, for example, introducing open metal sites and open non-metal sites[25–28], making narrow pores by controlling the interpenetration or alteration of the framework[29,30], doping metal centers into the framework[31], and pore surface modification by ligand functionalization[32–34]. The ligand functionalization method has been proven to be a facile way to tune the peculiarity of MOFs since the affinity between adsorbed guests and the host framework could be tuned without causing significant difference of the porous framework. Recently, the utilization of fluorinated linkers in MOFs construction has caught scientists' attention because of the unique properties of fluorous MOFs. It has been reported that the fluorous MOFs could reveal remarkable gas sorption capacities with the enhanced interactions between the fluorinated pore surface and gas molecules[35]. However, follow-up research found that not all fluorinated MOFs are beneficial to higher H$_2$ and CO$_2$ adsorption capacities, but is rather system-specific and differs from system to system[36–39]. In some cases, gas sorption amount of the desired MOFs had no obvious increase or even decreased. This might be attributed to the alternation of pore structure: the inserted functional groups may reduce the free pore volume. As a result, the effect of the fluorinated MOFs for gas sorption is complicated and systematic investigations should be proceeded to realize performance targeted rational design and construction.

In our efforts to construct functional porous MOFs, we have found that the reaction of Ni(II) anions with 2,4,6-tri(4-pyridinyl)-1,3,5-triazine (tpt) and o-phthalic acid (OPA) as co-ligand could result in highly porous frameworks. Furthermore, the decoration of pores surface and tuning of adsorption properties could be achieved by introducing different functional groups on the o-phthalic acid ligand. Herein, we report a new class of MOFs, TKL-101 to 107 (TKL = Tianjin Key Lab of Metal and Molecule Based Materials), with different functionalized
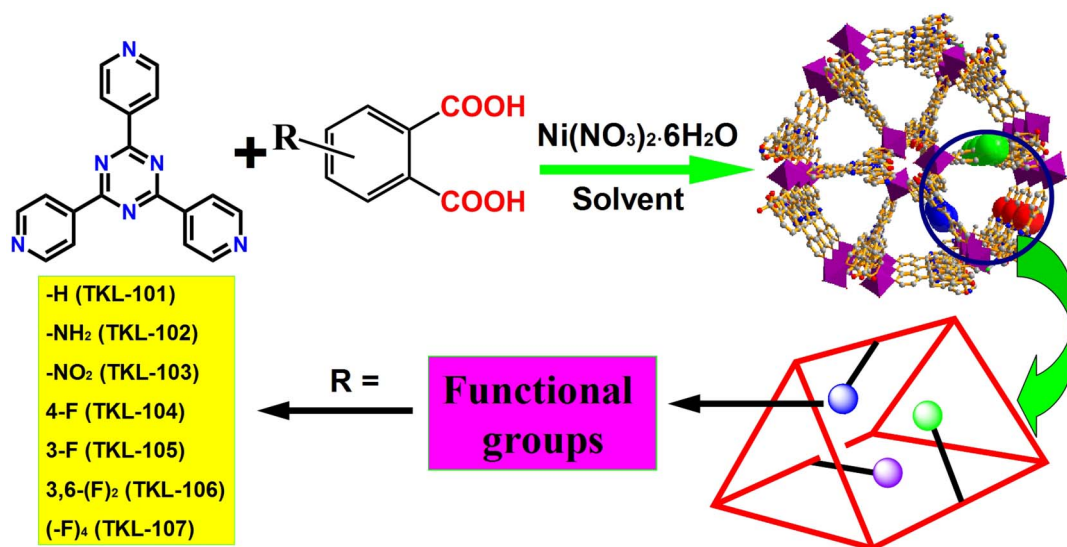
Figure 1 | General route for the synthesis of TKL MOFs.

(-NH₂, -NO₂, and -F) OPA as co-ligands (Figure 1). Interestingly, we found that the fluorination of the pore walls inside the framework could remarkably improve the stability of the MOFs materials, which could be reasonably explained by theoretical studies. Also, the gas adsorption properties studies revealed that all the fluorinated MOFs with different number and position of substituted fluorine atoms (TKL-104–TKL-107) reveal high surface areas and excellent ability for H_2 storage and CO_2 capture. Furthermore, to better explore the potential application of MOFs towards membrane-based CO_2 capture, TKL-107-doped mixed matrix membranes (MMMs) were prepared to test the potentiality of these materials for CO_2 separation.

Results

Synthesis. Solvothermal reaction of $Ni(NO_3)_2 \cdot 6H_2O$, tpt and OPA gave the crystals of TKL-101. By analyzing the coordination environment of OPA ligand inside the framework, we found that there were enough spaces inside the pores for the ligand functionalization. As a result, a series of OPAs with different functional groups including -NH₂, -NO₂, and –F, were chosen for the preparation of functionalized MOFs. Under similar conditions, functionalized TKL-102 to 107 were successfully synthesized.

Structure description. As the TKL series MOFs have similar structures, only TKL-101 is selected as an example to describe the structure in detail here. Crystallographic analysis reveals that TKL-101 crystallized in chiral space group of $P3_221$ or $P3_121$ at random, possessing a three dimensional (3D) porous framework with chiral channels. As shown in Figure 1, each Ni(II) ion is coordinated by three nitrogen atoms from three different tpt ligands, two carboxylate oxygen atoms from two different o-pathalate ions and one water molecule, resulting in a slightly distorted NiN_3O_3 octahedron geometry. Each o-pathalate ligand bridges two Ni(II) ions and each tpt ligand coordinates with three Ni(II) ions to generate an infinite 3D framework. The Ni–O/N bond lengths are in the range of 2.072(3) to 2.112(3) Å, and the O/N–Ni–O/N bond angles are in the range of 87.92(8) to 180.0(3)°, which are similar to those reported in related Ni(II) MOFs.

The framework structure of TKL-101 could be simplified into a rare 3, 5-connected chiral topology with the vertex symbol of (4.7^2) $(4^3.6^2.7^4.8)$ when considering the ligands and metal centers as three and five coordinated nodes[40], respectively (Figure 2). It should be noted that this unique topology could also be considered to be based on 3-coordinated uniform self-penetrating **twt** network topology[41] constructed from Ni(II) ions and tpt ligands as nodes, which is further interconnected by the OPA ligand. Crystals of TKL-101 crystallized in enantiomorphous chiral space groups, and its framework possesses three types of chiral helical chains. As shown in Figure 1, the tpt ligands are linked by Ni(II) ions to form A-type -tpt-Ni-tpt- double-helical chains (Figure 2, purple) with a pitch of 18.54 Å. Additionally, there exists the chiral helical tube, which is composed of B-type -tpt-Ni-tpt- helical chains (Figure 2, green), which are reinforced by the coordination of OPA ligands with Ni(II) to generate the C-type helical chain (Figure 2, red).

The network of TKL-101 contains channels running along the c axis, which have an opening size of $\sim 6.2 \times 6.2$ Å² (a × b) (Figure S2), excluding the van der Waals radius of atoms. After removal of solvent molecules filled in the pore space, the accessible volume of TKL-101 is 64.4%, as estimated using the SOLV function of PLATON software. Moreover, the benzene ring of OPA ligand point to the void of pitch between the A-type -tpt-Ni-tpt- double-helical chains. As a result, there is abundant space for the introduction of functional groups. Therefore, after decorating with different functional groups, the total solvent-accessible volumes of the framework of TKL-101 to 107 were estimated to be in the range of 60%–65% with little discount. The structural characteristic of TKL MOFs thus allows a systematic variation of functional groups to achieve open frameworks with multiple functions.

Powder X-ray diffraction. Powder X-ray diffraction (PXRD) data analysis was conducted to confirm the phase purity of TKL-101–TKL-107 (Figure S11–S17). The patterns from the as-synthesized bulk products closely match the simulated ones from single-crystal analysis, suggesting the pure solid-state phases of these samples. Also, all the solvent-exchanged samples are crystalline. However, after the degas treatment, TKL-101-104 lost their long range order, and only TKL-105, TKL-106 and TKL-107 still present high crystallinity after adsorption experiments, as evidenced by the PXRD patterns, which indicate good stability of the fluorine decorated frameworks after the removal of guest solvent molecules. Furthermore, comparing the PXRD patterns of TKL-104 with those of TKL-105 to 107, it is obvious that the functionalization with F atom at 3-position of OPA is much more efficient than at 4-position for structure stabilization purpose.

Theoretical study. From the above mentioned results, it revealed that F atoms played the key role in improving the framework stability. To better understand the stability mechanism of the fluorine-functionalized MOFs, theoretical calculations were performed on the
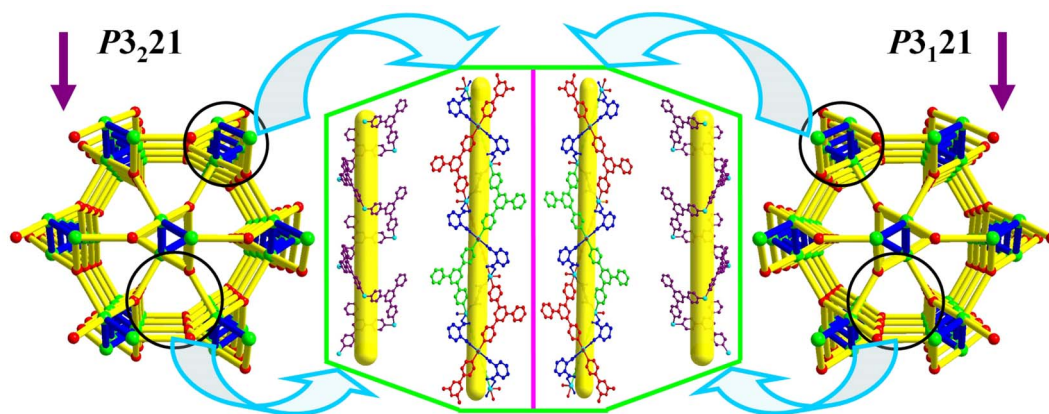
Figure 2 | Chiral topologies of the TKL MOFs and helical chains surrounded channels inside the frameworks.

model compounds, TKL-101, TKL-104, TKL-105, TKL-106 and TKL-107. DFT calculations were carried out with the Gaussian 09 package using wB97XD functional and Mayer bond order, which appeared to be a reasonable interpretation, was analyzed by calculation based on the crystal structures without theoretical optimization (Table S3 and S4). The result revealed that the total Mayer bond order of Ni based coordination bonds is 2.374 for TKL-101 and 2.385 for TKL-104, which are very close to that of TKL-105 (2.378), TKL-106 (2.347) and TKL-107 (2.345). But for TKL-105–TKL-107, there might exist additional weak interactions (Figure 3 and S18) between F atoms, mainly from the 3-position in OPA, and H atoms from tpt ($d_{3\text{-F-H}} = 2.402$–2.566 Å) and Ni center ($d_{3\text{-F-Ni}} = 4.547$–$4.650$ Å). Moreover, the total Mayer bond order of fluorine based weak interactions is 0.090 (F···H, 0.065 and F···Ni, 0.025) for TKL-105, 0.134 (F···H, 0.086 and F···Ni, 0.048) for TKL-106 and 0.128 (F···H, 0.074 and F···Ni, 0.054) for TKL-107, which could further confirm the important roles of the 3-F caused weak interactions in stabilizing the frameworks. As for the 4-F decorated TKL-104, there were almost no interaction between fluorine and ambient atoms, because of the long distance ($d_{4\text{-F-H}} = 4.892$ Å, $d_{4\text{-F-Ni}} = 7.027$ Å) between them. On the other hand, the total Mayer bond order of Ni and F based interactions were calculated. The results also proved higher stability of TKL-105 (2.567), TKL-106 (2.556) and TKL-107 (2.578) than that of TKL-101 (2.534) and TKL-104 (2.495). As a result, it could be deduced that the additional weak

interactions between the introduced fluorine and ambient atoms inside the framework might be one essential factor in stabilizing the framework structures of these MOFs with 3-F decorated pores.

Porosity characterization. Nitrogen gas adsorption experiments at 77 K were performed for the pore characterization of these materials. All the F decorated MOFs show higher porosity compared with others (Figure 4a and Figure S21), and the details are summarized in Table 1. As shown in Figure 4a, N_2 sorption isotherms of TKL-104–TKL-107 present a type-I kind behavior, indicating the microporosity of these MOFs. These sorption curves were analyzed by using the Brunauer–Emmett–Teller (BET) and Langmuir methods. The results demonstrate that the fluorine-functionalized TKL-104–TKL-107 are highly porous, with BET and Langmuir surface areas ranging from 1131 to 1636 $m^2\ g^{-1}$ and 1500 to 2171 $m^2\ g^{-1}$, respectively, and pore volumes from 0.56 to 0.80 $cm^3\ g^{-1}$. Taking the different OPA ligands used into account, it is obvious that specific surface areas and pore volumes can be controlled by the different number and position of fluorine atoms inside the frameworks. Also, the relatively lower surface areas and pore volumes of TKL-104 than those of TKL-105 to 107 suggest the relatively lower stability of 4-F decorated framework than that with 3-F inside the frameworks. These observations agree well with the evidence of their PXRD patterns mentioned above. Pore size distribution curves (Figure 4b) for these materials were studied by analyzing the N_2 sorption isotherms using Horvath- Kawazoe method (HK). It can be found that these
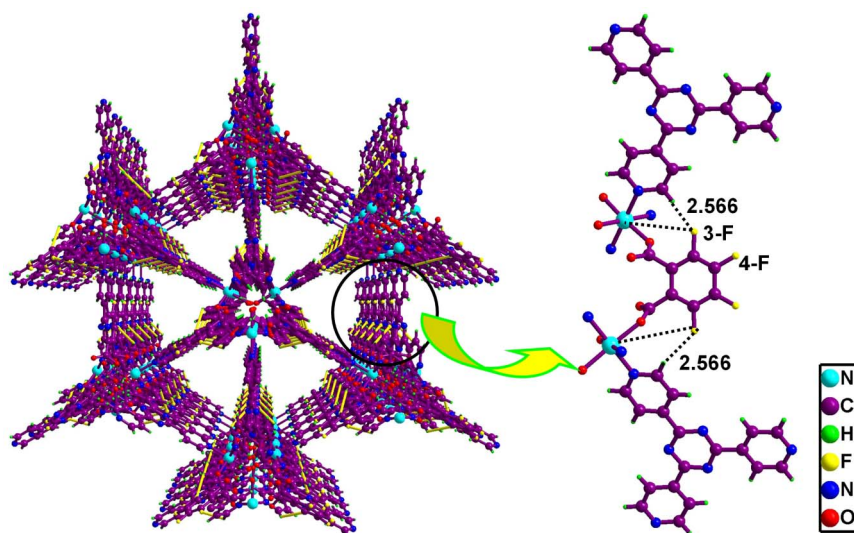

Figure 3 | Schematic diagram of the possible weak interactions between the introduced fluorine and ambient atoms inside the framework of TKL-107 (yellow bonds). Distances of close contact, in Å, are marked in the figure.
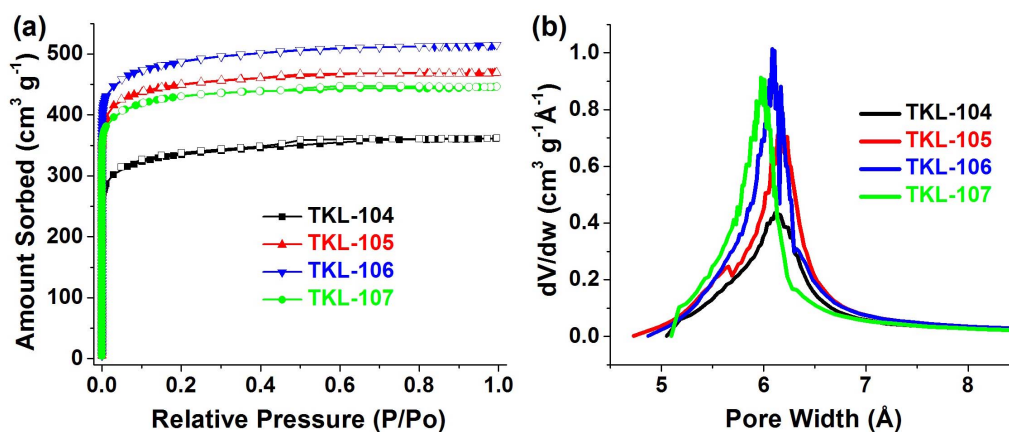
Figure 4 | N$_2$ sorption isotherms (a) and pore size distributions (b) for TKL-104–TKL-107.

fluorine-functionalized MOFs all show micropore size distributions mainly around 6.0; and the pore size ranking is TKL-105 (6.2 Å) > TKL-106 (6.1 Å) > TKL-107 (6.0 Å).

Hydrogen adsorption. In order to comprehend the hydrogen storage properties of the fluorine-functionalized MOFs under low pressure, H$_2$ adsorption and desorption isotherms (Figure 5a) were measured at 77 and 87 K, respectively. All the sorption curves display type I adsorption behaviors and no hysteresis was observed. The fluorinated MOFs can adsorb a considerable amount of H$_2$ at 77 K and 1.2 bar, that is 196 cm^3 g^{-1} (1.75 wt%) for TKL-104, 218 cm^3 g^{-1} (1.95 wt%) for TKL-105, 236 cm^3 g^{-1} (2.1 wt%) for TKL-106 and 225 cm^3 g^{-1} (2.0 wt%) for TKL-107. These H$_2$ adsorption capacities are comparable to many reported MOFs (Table S5) like MOF-5[6], MOF-177[42], NOTT-400[43], and CPF-6[27]. Furthermore, it should be noticed that the micropore size distributions of TKL-104–TKL-107 involved above are all around 6.0 Å, just close to the size about two H$_2$ molecules (2 × 2.8 Å), this may help enhancing the interaction between the H$_2$ molecules and the framework and benefit the hydrogen storage performances. On the other hand, the amount of H$_2$ molecules adsorbed in each lattice volume was calculated to be 14.9 for TKL-104, 16.6 for TKL-105, 18.6 for TKL-106, and 18.8 for TKL-107. Considering the decreasing cell volume and similar porosity of TKL-104–TKL-107 (Table S1), these results indicate the positive effect of fluorine to hydrogen storage capacity in this MOF system. Finally, it is also obvious that the H$_2$ adsorption properties can be adjusted by controlling the fluorinating inside the frameworks.

Carbon dioxide capture. CO$_2$ adsorption isotherms were measured to explore the ability of CO$_2$ capture of these fluorine-functionalized MOFs. As shown in Figure 5b, TKL-107 has a considerable ability of CO$_2$ capture, that is, 150 cm^3 g^{-1} (29.5 wt%) at 273 K and 1.2 bar. TKL-105 and TKL-106 can also adsorb a large amount of CO$_2$ (105 cm^3 g^{-1} and 126 cm^3 g^{-1} at 273 K and 1.2 bar, respectively).

The CO$_2$ molecules adsorbed per cell volume was calculated to be 8.0, 9.9, and 12.5 for TKL-105 to TKL-107, respectively. The CO$_2$ uptake order (TKL-107 > TKL-106 > TKL-105) indicates that the CO$_2$ adsorptions of these materials could be tuned by the degree of the F modification in the framework: the more fluoride atoms the framework possesses, the higher uptake capacity it could achieve. However, in the case of TKL-104, only an uptake of 33 cm^3 g^{-1} was observed at 273 K. This obvious decrease in CO$_2$ uptake might be attributed to the framework collapse, well supported by the PXRD patterns comparison. Also, the fluorine-functionalized TKL MOFs exhibit good selective adsorption of CO$_2$ over CH$_4$ and N$_2$ (Figure S26). At 273 K and 1 bar, the CO$_2$/CH$_4$ selectivity is about 4.5 : 1 (v/v) for TKL-107, 4.4 : 1 (v/v) for TKL-106 and 4.1 : 1 (v/v) for TKL-105. On the other hand, the initial slopes of the adsorption isotherms were calculated and the ratios of these slopes could also be used to estimate the adsorption selectivity at very low pressure (Figure S23–25)[44]. The calculated CO$_2$/N$_2$ selectivity from these data is about 13.8 : 1 for TKL-107, 15.0 : 1 for TKL-106, and 15.8 : 1 for TKL-105, respectively, which were in accord with the isosteric heats (Figure S20). Using the same method, the CO$_2$/CH$_4$ selectivities were calculated to be 5.0 : 1, 4.6 : 1, and 4.8 : 1, respectively. The high adsorption capacity and selectivity towards CO$_2$ make these fluorine-functionalized TKL MOFs good candidates for the capture and separation of CO$_2$.

High pressure adsorptions. To further study the total capacity of H$_2$, CO$_2$, and CH$_4$ adsorption, high pressure adsorption experiments for TKL-106 and TKL-107 were conducted on these gases. Figure 5c shows that excess uptake of H$_2$ at 77 K for TKL-106 and TKL-107 are 6.24 wt% and 4.0 wt% till 66 bar, respectively. Also, CO$_2$ saturated uptake at 273 K is 34.2% for TKL-106 and 42.5 wt% for TKL-107 till 30 bar and CH$_4$ uptake at 273 K is 21.4% for TKL-106 and 20.1 wt% for TKL-107 till 66 bar, respectively (Figure 5d). These results reveal that TKL-106 and TKL-107 can be good candidates for energy gas storage and greenhouse gas capture applications.

MOFs	S$_{BET}$ (m^2 g^{-1})	S$_{Langmuir}$	Pore volume (cm^3 g^{-1})	H$_2$ uptake (wt%)	CO$_2$ uptake (cm^3 g^{-1})	CH$_4$ uptake (cm^3 g^{-1})
TKL-104	1131	1503	0.56	1.75[a]	32.6[c]	6.5[d]
TKL-105	1509	2002	0.73	1.95[a]	105[c]	28.9[d]
TKL-106	1636	2171	0.80	2.11[a], 6.24[b]	123[c]	25.8[d]
TKL-107	1454	1917	0.69	2.01[a], 4.0[b]	150[c]	33.8[d]

Table 1 | Gas uptake properties of TKL-104–TKL-107

[a]Low pressure H$_2$ uptake at 77 K.
[b]High pressure H$_2$ uptake at 77 K.
[c]Low pressure CO$_2$ uptake at 273 K.
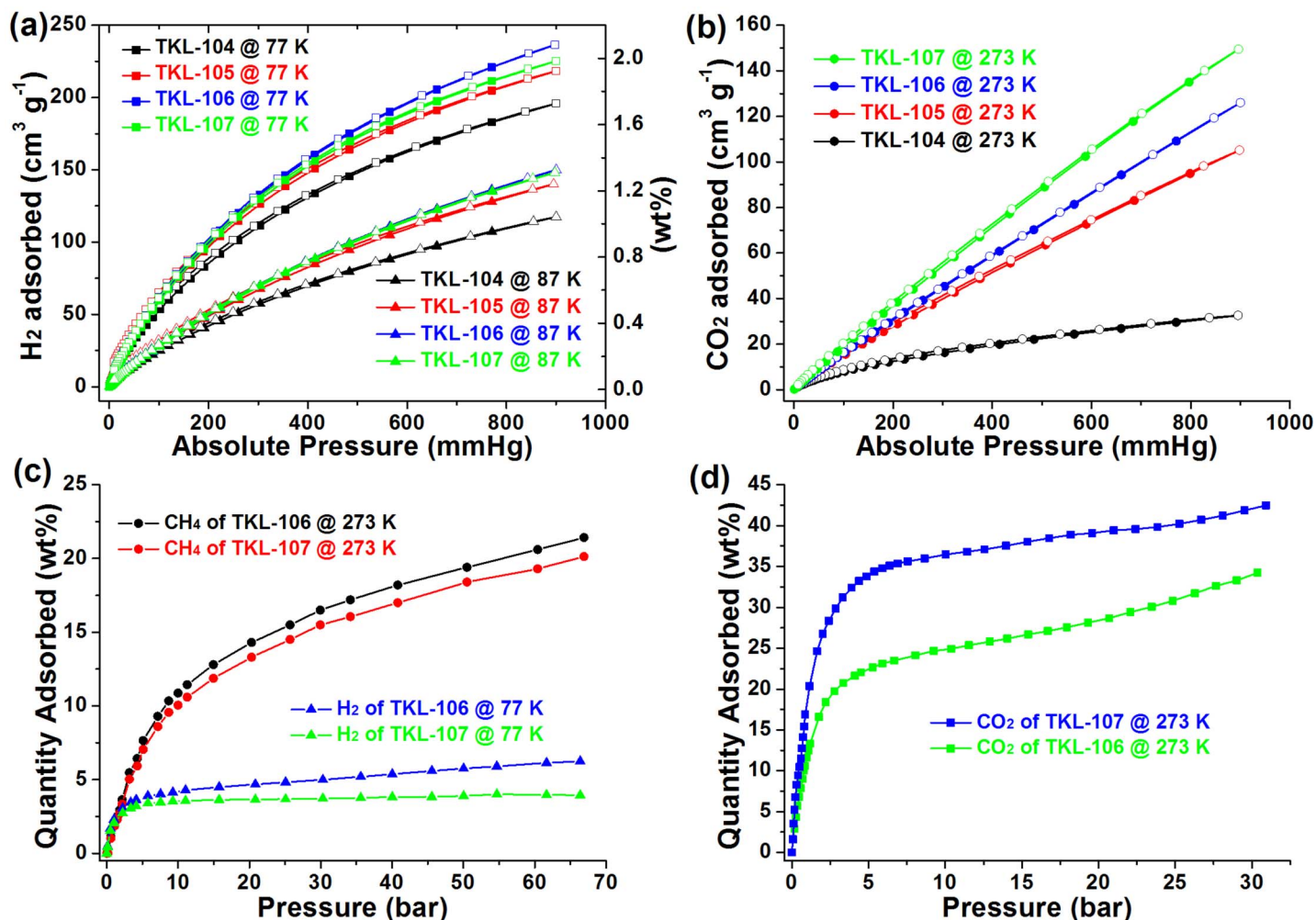[d]Low pressure CH$_4$ uptake at 273 K.

Figure 5 | (a) and (c) H_2 adsorption isotherms at 77 K; (b) CO_2 adsorption isotherms at 273 K and low pressure; (d) High pressure CO_2 and CH_4 adsorption isotherms at 273 K.

Gas permeation experiments. As the membrane-based separation processes might provide efficient and economical solution for CO_2 capture and purification[45], TKL-107 filled MMMs were prepared and their CO_2 separation performances were tested. The preparing process of MMMs and apparatus for testing flat-sheet dense membranes was shown in Figure S27–S29. The ideal and mixed CO_2/CH_4 selectivity (α) was calculated by: $\alpha = P_{CO2}/P_{CH4}$. The permeability and selectivity values at different loadings are plotted in Figure 6. It can be seen that along with the increase of TKL-107 loading, both the ideal selectivity and mixed-gas selectivity values reach a maximum of 64.6 and 50.3 at 20% TKL-107 loading, respectively, and the permeability values present a nonlinear upward trend. Similar trends have been observed for other MOFs-filled mixed matrix membranes[46,47]. At low MOF loading, the superior sieving ability of MOF as well as good polymer/filler adhesion ensures higher permeability and selectivity than pristine polymeric membrane. However, non-ideal polymer/filler interfacial defects caused by particle agglomeration may occur at high MOF loading, leading to the accelerated enhancement of permeability and the decay of selectivity[48]. More importantly, the testing results for TKL-107-filled MMMs rival other MOFs-doped MMMs with Matrimid as the benchmark polymer matrix[46,49,50], showing a promising potential of TKL-107 as filler in MMMs.

Discussion

The design and synthesis of a new series of functionalized MOFs have been reported. Gas adsorption properties of these MOFs were

systemically studied at low and high pressure. Among the reported MOFs, the ones with fluoride decorated pore walls (TKL-104–TKL-107) exhibit high specific surface areas and uptake of H_2 and CO_2, which might be applicable in energy storage and environment improvement. More importantly, it could be found that the stability and adsorption properties could be improved when fluorine was introduced into the framework through ligand functionalization. Theoretical analyses of these MOFs structures could also clarify the pivotal roles of fluorine in improving the stability of the frameworks. Additionally, the CO_2/CH_4 permeation experiments were performed with TKL-107-filled MMMs and it reaches a maximum of 64.6 and 50.3 for the selectivity at 20% loading. These properties make it a promising candidate for CO_2/CH_4 separation. Further studies on the effect of ligand functionalization to the gas adsorptions and separation properties of MOFs will be in the schedule of our future research.

Methods

Synthesis of TKL-MOFs. The tpt ligand was synthesized according to the reported method[51]. TKL-101 was prepared by solvothermal reaction of $Ni(NO_3)_2 \cdot 6H_2O$ (0.1 mmol), OPA (0.05 mmol), tpt (0.05 mmol) in DMF (4 ml) at 100°C for 2 days. TKL-102–TKL-107 were obtained using a similar procedure (see ESI for more details).

Characterization. Single-crystal X-ray diffraction measurement for TKL-101 to 103 was carried out on a Rigaku Saturn70 diffractometer at 113 K, and diffraction data for TKL-104 to 107 was collected on a Rigaku Saturn724+ diffractometer at 113 K. The determinations of unit cell parameters and data collections were performed with Mo
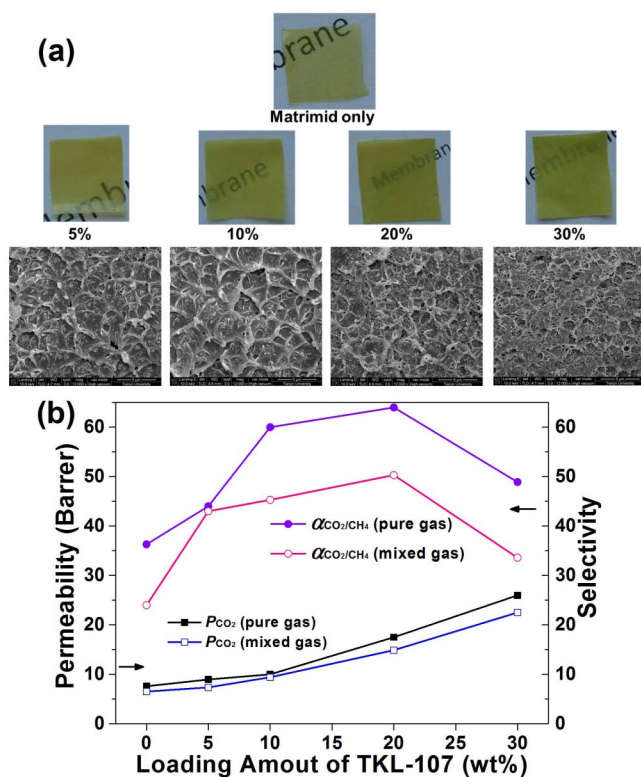
Figure 6 | (a) Photos and SEM images of the mixed membranes with different doping amount of TKL-107. (b) CO_2/CH_4 selectivity and permeability trend of the TKL-107 MMMs towards pure gas and mixed gas.

Kα radiation (λ = 0.71073 Å), and unit cells were obtained with least-squares refinements. The program SAINT was used for integration of the diffraction profiles. Semiempirical absorption corrections were applied using the SADABS program. The structures were solved by direct methods using the SHELXS program of the SHELXTL package and refined with SHELXL. Nickel atoms were found from E maps, and other non-hydrogen atoms were located in successive difference Fourier syntheses. The final refinements were performed by full matrix least-squares methods with anisotropic thermal parameters for non-hydrogen atoms on F^2. The hydrogen atoms were added theoretically, riding on the concerned atoms, and refined with fixed thermal factor except for H_2O molecules. The disorders were treated by occupancies refinement of the disordered atoms. The contribution of disordered solvent molecules were treated using the SQUEEZE procedure implemented in PLATON[52]. CCDC 924082-924088 contains the supplementary crystallographic data for this paper. These data can be obtained free of charge from the Cambridge Crystallographic Data Centre via www.ccdc.cam.ac.uk/data_re-quest/cif.

Sorption measurements. Low pressure gas adsorption measurements were conducted using an ASAP2020M gas adsorption analyzer and UHP-grade gases were used in measurements. Nitrogen isotherm measurements were preceded at 77 K in a liquid nitrogen bath. The hydrogen sorption isotherms were collected at 77 K in a liquid nitrogen bath and 87 K in a liquid argon bath. Carbon dioxide adsorptions were tested at 195 K, 273 K and 298 K. Before measurements, the samples were soaked in CH_2Cl_2 for several days to exchange the guest solvents and then filtrated and dried at room temperature. The dry samples were loaded in sample tubes and activated under high vacuum (less than 10^{-5} Torr) at 40°C. About 100 mg of degassed samples were used for gas sorption measurements, and the weight of each sample was recorded before and after outgassing to confirm the removal of guest molecules. The outgassing procedure was repeated on the same sample between several experiments for 0.5–1 h. High pressure gas adsorption measurements were performed using a PCTpro-2000 high pressure adsorption analyzer and UHP-grade gases were used in measurements. The samples used in the measurement were first degased on the degas station of ASAP 2020 M gas adsorption analyzer then transferred to the sample holder of high pressure adsorption analyzer and further degased at 40°C for five hours before the measurements.

Fabrication of TKL-polymer MMMs. Before fabrication, a sample of TKL-107 was fully grinded. Then, TKL-107 (0.020 g/0.040 g/0.080 g/0.120 g) were dispersed in DMF (1.6 g) and bath sonicated for 1 h to form the TKL-107 contained suspension. Subsequent dropping a solution containing Matrimid 5218 (0.380 g/0.360 g/0.320 g/ 0.280 g) and DMF (6.0 g) into the formal suspension gave the original mixed solution

for the membranes. The mixed homogeneous solutions were then cast onto clean glass sheets and dried at 60°C for 12 h, 100°C for another 12 h and cooled to room temperature. Finally, a series of TKL-107-MMMs (5 wt%/10 wt%/20 wt%/30 wt%) were obtained, after solvent exchanged using methanol for three times per 12 h. (scheme S1) Additionally, 0.400 g Matrimid 5218 were dissolved in 7.6 g DMF as a contrast. The average membrane thickness is 60 ∼ 70 μm (Figure S28) and before testing, the membranes were dried for 24 h at 50°C under vacuum.

Gas permeation experimental conditions. Gas permeation experiments were conducted at 25°C based on the conventional constant pressure/variable volume technique. The pressure of feed gas (CO_2, CH_4, or mixed gas CO_2/CH_4 = 20/80 vol%) and sweeping gas (N_2) were maintained at 2 bar and 0.1 bar, respectively. The compositions of the feed, retentate, and permeate were measured using Agilent 6820 gas chromatography equipped with a thermal conductive detector (TCD). The permeability (P_i, Barrer) of either gas was obtained from the average value of at least twice measurements, by using the equation: $P_i = Q_i l/\Delta p_i A$, where Q_i is the volumetric flow rate of gas 'i' (cm^3/s) at standard temperature and pressure (STP), Δp_i is the transmembrane pressure difference (cmHg), and A is the effective membrane area, 12.56 cm^2.

1. Suh, M. P., Park, H. J., Prasad, T. K. & Lim, D.-W. Hydrogen storage in metal-organic frameworks. *Chem. Rev.* **112**, 782–835 (2012).
2. Sumida, K. *et al.* Carbon dioxide capture in metal-organic frameworks. *Chem. Rev.* **112**, 724–781 (2012).
3. Zhou, H. C., Long, J. R. & Yaghi, O. M. Introduction to metal-organic frameworks. *Chem. Rev.* **112**, 673–674 (2012).
4. Horike, S., Shimomura, S. & Kitagawa, S. Soft porous crystals. *Nat. Chem.* **1**, 695–704 (2009).
5. Wang, X.-L. *et al.* Bottom-up synthesis of porous coordination frameworks: apical substitution of a pentanuclear tetrahedral precursor. *Angew. Chem. Int. Ed.* **48**, 5291–5295 (2009).
6. Lu, W. *et al.* Porous polymer networks: synthesis, porosity, and applications in gas storage/separation. *Chem. Mater.* **22**, 5964–5972 (2010).
7. Ma, H., Ren, H., Meng, S., Sun, F. & Zhu, G. Novel Porphyrinic Porous Organic Frameworks for High Performance Separation of Small Hydrocarbons. *Sci. Rep.* **3**, 2611; DOI:10.1038/srep02611 (2013).
8. El-Kaderi, H. M. *et al.* Designed synthesis of 3D covalent organic frameworks. *Science* **316**, 268–272 (2007).
9. Kuhn, P., Forget, A. l., Su, D., Thomas, A. & Antonietti, M. From microporous regular frameworks to mesoporous materials with ultrahigh surface area: dynamic reorganization of porous polymer networks. *J. Am. Chem. Soc.* **130**, 13333–13337 (2008).
10. Li, H., Eddaoudi, M., O'Keeffe, M. & Yaghi, O. M. Design and synthesis of an exceptionally stable and highly porous metal-organic framework. *Nature* **402**, 276–279 (1999).
11. Gong, Y.-N. *et al.* Counter-cation modulation of hydrogen and methane storage in a sodalite-type porous metal-organic framework. *Chem. Commun.* **48**, 12002–12004 (2012).
12. Nugent, P. *et al.* Porous materials with optimal adsorption thermodynamics and kinetics for CO_2 separation. *Nature* **495**, 80–84 (2013).
13. Li, J.-R., Sculley, J. & Zhou, H.-C. Metal-organic frameworks for separations. *Chem. Rev.* **112**, 869–932 (2012).
14. Li, S.-L., Lan, Y.-Q., Sakurai, H. & Xu, Q. Unusual regenerable porous metal–organic framework based on a new triple helical molecular necklace for separating organosulfur compounds. *Chem. Eur. J.* **18**, 16302–16309 (2012).
15. Guo, H., Zhu, G., Hewitt, I. J. & Qiu, S. "Twin copper source" growth of metal–organic framework membrane: $Cu_3(BTC)_2$ with High Permeability and Selectivity for Recycling H_2. *J. Am. Chem. Soc.* **131**, 1646–1647 (2009).
16. Lee, J. *et al.* Metal-organic framework materials as catalysts. *Chem. Soc. Rev.* **38**, 1450–1459 (2009).
17. Cui, Y., Yue, Y., Qian, G. & Chen, B. Luminescent functional metal–organic frameworks. *Chem. Rev.* **112**, 1126–1162 (2011).
18. Du, D.-Y. *et al.* An unprecedented (3,4,24)-connected heteropolyoxozincate organic framework as heterogeneous crystalline Lewis acid catalyst for biodiesel production. *Sci. Rep.* **3**, 2616; DOI:10.1038/srep02611 (2013).
19. Shan, X.-C. *et al.* A multi-metal-cluster MOF with Cu_4I_4 and Cu_6S_6 as functional groups exhibiting dual emission with both thermochromic and near-IR character. *Chem. Sci.* **4**, 1484–1489 (2013).
20. Gong, Y.-N. & Lu, T.-B. Fast detection of oxygen by the naked eye using a stable metal-organic framework containing methyl viologen cations. *Chem. Commun.* **49**, 7711–7713 (2013).
21. Sun, C.-Y. *et al.* Chiral nanoporous metal-organic frameworks with high porosity as materials for drug delivery. *Adv. Mater.* **23**, 5629–5632 (2011).
22. Horcajada, P. *et al.* Metal-organic frameworks in biomedicine. *Chem. Rev.* **112**, 1232–1268 (2012).
23. Farha, O. K. *et al.* De novo synthesis of a metal-organic framework material featuring ultrahigh surface area and gas storage capacities. *Nat. Chem.* **2**, 944–948 (2010).
24. Furukawa, H. *et al.* Ultrahigh porosity in metal-organic frameworks. *Science* **329**, 424–428 (2010).

25. Hong, D.-Y., Hwang, Y. K., Serre, C., Ferey, G. & Chang, J.-S. Porous chromium terephthalate MIL-101 with coordinatively unsaturated sites: surface functionalization, encapsulation, sorption and catalysis. *Adv. Funct. Mater.* **19**, 1537–1552 (2009).

26. Wang, X.-J. *et al.* A rationally designed nitrogen-rich metal-organic framework and its exceptionally high CO_2 and H_2 uptake capability. *Sci. Rep.* **3**, 1149; DOI:10/1038/srep01149 (2013).

27. Lin, Q., Wu, T., Zheng, S.-T., Bu, X. & Feng, P. Single-walled polytetrazolate metal-organic channels with high density of open nitrogen-donor sites and gas uptake. *J. Am. Chem. Soc.* **134**, 784–787 (2012).

28. Chang, Z. *et al.* Rational construction of 3D pillared metal–organic frameworks: synthesis, structures, and hydrogen adsorption properties. *Inorg. Chem.* **50**, 7555–7562 (2011).

29. Shekhah, O. *et al.* Controlling interpenetration in metal-organic frameworks by liquid-phase epitaxy. *Nat. Mater.* **8**, 481–484 (2009).

30. Ghosh, S. K., Kaneko, W., Kiriya, D., Ohba, M. & Kitagawa, S. A bistable porous coordination polymer with a bond-switching mechanism showing reversible structural and functional transformations. *Angew. Chem. Int. Ed.* **47**, 8843–8847 (2008).

31. Dinca, M. & Long, J. R. High-enthalpy hydrogen adsorption in cation-exchanged variants of the microporous metal-organic framework $Mn_3[(Mn_4Cl)_3(BTT)_8(CH_3OH)_{10}]_2$. *J. Am. Chem. Soc.* **129**, 11172–11176 (2007).

32. Zhao, Y. *et al.* Enhancing gas adsorption and separation capacity through ligand functionalization of microporous metal–organic framework structures. *Chem. Eur. J.* **17**, 5101–5109 (2011).

33. Zheng, B., Bai, J., Duan, J., Wojtas, L. & Zaworotko, M. J. Enhanced CO_2 binding affinity of a high-uptake rht-type metal-organic framework decorated with acylamide groups. *J. Am. Chem. Soc.* **133**, 748–751 (2011).

34. Deng, H. *et al.* Multiple functional groups of varying ratios in metal-organic frameworks. *Science* **327**, 846–850 (2010).

35. Yang, C., Wang, X. & Omary, M. A. Fluorous Metal−Organic Frameworks for High-Density Gas Adsorption. *J. Am. Chem. Soc.* **129**, 15454–15455 (2007).

36. Pachfule, P., Chen, Y., Jiang, J. & Banerjee, R. Fluorinated metal–organic frameworks: advantageous for higher H_2 and CO_2 adsorption or not? *Chem. Eur. J.* **18**, 688–694 (2012).

37. Pachfule, P., Chen, Y., Sahoo, S. C., Jiang, J. & Banerjee, R. Structural Isomerism and Effect of Fluorination on Gas Adsorption in Copper-Tetrazolate Based Metal Organic Frameworks. *Chem. Mater.* **23**, 2908–2916 (2011).

38. Pachfule, P., Das, R., Poddar, P. & Banerjee, R. Solvothermal Synthesis, Structure, and Properties of Metal Organic Framework Isomers Derived from a Partially Fluorinated Link. *Crystal Growth & Design* **11**, 1215–1222 (2011).

39. Pachfule, P., Das, R., Poddar, P. & Banerjee, R. Structural, magnetic, and gas adsorption study of a series of partially fluorinated metal-organic frameworks (HF-MOFs). *Inorg. Chem.* **50**, 3855–3865 (2011).

40. Chang, Z., Zhang, D.-S., Hu, T.-L. & Bu, X.-H. Synthesis, structure and properties of microporous metal–organic frameworks constructed from Ni(II)/Cd(II), Tpt and H_4bpta. *Inorg. Chem. Commun.* **14**, 1082–1085 (2011).

41. Abrahams, B. F. *et al.* Ni(tpt)(NO$_3$)$_2$–A three-dimensional network with the exceptional (12,3) topology: a self-entangled single net. *Angew. Chem. Int. Ed.* **38**, 1475–1477 (1999).

42. Chae, H. K. *et al.* A route to high surface area, porosity and inclusion of large molecules in crystals. *Nature* **427**, 523–527 (2004).

43. Ibarra, I. A. *et al.* Highly porous and robust scandium-based metal-organic frameworks for hydrogen storage. *Chem. Commun.* **47**, 8304–8306 (2011).

44. An, J., Geib, S. J. & Rosi, N. L. High and selective CO_2 uptake in a cobalt adeninate metal−organic framework exhibiting pyrimidine- and amino-decorated pores. *J. Am. Chem. Soc.* **132**, 38–39 (2009).

45. Bernardo, P., Drioli, E. & Golemme, G. Membrane gas Separation: a review/state of the art. *Ind. Eng. Chem. Res.* **48**, 4638–4663 (2009).

46. Bushell, A. F. *et al.* Gas permeation parameters of mixed matrix membranes based on the polymer of intrinsic microporosity PIM-1 and the zeolitic imidazolate framework ZIF-8. *J. Membr. Sci.* **427**, 48–62 (2013).

47. Song, Q. *et al.* Zeolitic imidazolate framework (ZIF-8) based polymer nanocomposite membranes for gas separation. *Energy Environ. Sci.* **5**, 8359–8369 (2012).

48. Moore, T. T. & Koros, W. J. Non-ideal effects in organic–inorganic materials for gas separation membranes. *J. Mol. Struct.* **739**, 87–98 (2005).

49. Perez, E. V., Balkus, K. J. Jr., Ferraris, J. P. & Musselman, I. H. Mixed-matrix membranes containing MOF-5 for gas separations. *J. Membr. Sci.* **328**, 165–173 (2009).

50. Hu, J. *et al.* Mixed-Matrix Membrane Hollow Fibers of Cu$_3$(BTC)$_2$ MOF and polyimide for gas separation and adsorption. *Ind. Eng. Chem. Res.* **49**, 12605–12612 (2010).

51. Chang, Z., Zhang, D.-S., Hu, T.-L. & Bu, X.-H. Microporous metal−organic framework based on supermolecular building blocks (SBBs): structure analysis and selective gas adsorption properties. *Cryst. Growth Des.* **11**, 2050–2053 (2011).

52. Spek, A. Single-crystal structure validation with the program PLATON. *J. Appl. Crystallogr.* **36**, 7–13 (2003).

Acknowledgments

Author contributions

X.-H.B. designed the study. D.-S.Z. and Z.H.-X. performed most of the experiments and characteristics. Y.-F.L. and Z.-Y.J. made the MOF mixed matrix membranes, as well as the gas permeation experiment. Q.C. carried out the sorption measurements. Y.-H.Z. performed the theoretical calculations. J.-R.L. and T.-L.H. joined in the discussions and analyses. D.-S.Z., Z.C. and X.-H.B. prepared the manuscript and all authors reviewed the manuscript.

Additional information

Supplementary information accompanies this paper at http://www.nature.com/scientificreports

Competing financial interests: The authors declare no competing financial interests.

How to cite this article: Zhang, D.-S. *et al.* Fluorous Metal-Organic Frameworks with Enhanced Stability and High H_2/CO_2 Storage Capacities. *Sci. Rep.* **3**, 3312; DOI:10.1038/srep03312 (2013).